Research Article

J. Electrochem. Sci. Technol., **2023**, *14(1), 38-50*

Design and Analysis of Spider Bionic Flow Field for Proton Exchange Membrane Fuel Cell

Jian Yao, Fayi Yan*, and Xuejian Pei

School of Mechanical and Electronic Engineering, Shandong Jianzhu University, Jinan 250101, China

ABSTRACT

Proton exchange membrane fuel cell (PEMFC) is a portable and clean power generation device. The structural arrangement of the flow field has a significant influence on the delivery efficiency of PEMFC. In this article, a new bionic flow channel is designed based on the inspiration of a spider shape. The branch channel width and branch corner are studied as the focus, and its simulation is carried out by the method of computational fluid dynamics (CFD). The results show that when channel width/rib width and corner of the branch are 1.5 and 130°, respectively, it is the best numerical combination and the cell comprehensive performance is excellent. The final model using this numerical combination is compared with the traditional flow channel model to verify the advancement of this scheme.

Keywords : Proton Exchange Membrane Fuel Cell, Spider Bionic Flow Field, Oxygen Concentration, Water Content

Received : 28 June 2022, Accepted : 27 August 2022

1. Introduction

In response to the traditional energy problem such as renewable slow speed, and the environment dirtier, people have been trying to find a kind of high energy utilization of alternative energy sources [1-3]. In recent years, hydrogen energy has received more and more attention and has become an energy star that countries are competing to develop. Many countries have developed hydrogen development strategies, and PEMFC is an important product for carrying hydrogen energy. PEMFC has been gradually applied on many occasions including in automobiles, forklifts, and portable power supplies due to its pollution-free products and small space occupancy [4-8]. The bipolar plate is the "skeleton" of the battery pack, responsible for the distribution of reaction gas, collection of conduction current, and discharge of excess heat and water. The channel structure in the bipolar plate can control the flow state of the gas. The rational channel design directly affects the global efficiency of the fuel cell [9-15].

Because the channel structure plays a decisive role in the battery performance, its reasonable configuration is an important breakthrough to improve the output power. In addition to the structural improvement of the traditional channel, the new channel has attracted more and more attention from scholars from all over the world, and the bionic flow channel is one of them [16-19]. At present, most bionic flow channels remain in leaf and tree structures. Iranzo and Zhang *et al.* conducted a comparative analysis on a variety of bionic flow channels including leaf and lung structures [20,21], and the results showed that compared with traditional flow channels, bionic flow channels have more efficient water management and great development potential. Badduri *et al.* [22] compared and analyzed the bionic blade with the pulmonary bionic flow channel and the triple serpentine flow channel, and compared with the other two structures, the bionic blade flow channel had better performance and significantly improved the output power. Chen *et al.* [23] believed that the unique tree-like and lung-like structures in nature were natural heat and mass transfer channels, so they designed a new type of flow channel based on the vein structure and carried out a simulation analysis. The results showed that when the current density is higher than 0.6 A/

*E-mail address: yanfayi@sdjzu.edu.cn

DOI: https://doi.org/10.33961/jecst.2022.00479

cm^2, the advantage of the bionic flow field is more conspicuous, and the branching structure makes the oxygen distribution more well-proportioned. Unlike the former, such as Zhang [24] according to animals nest design a honeycomb type bionic structure flow channel, and exploring the gas diffusion layer (GDL) thickness and porosity affect the performance of PEMFC, the results show that honeycomb flow channel can improve the three-phase interface oxygen distribution uniformity, but too much of the branch, prone to "flooding" phenomenon. In contrast, although the bionic structure of the spider web proposed by Xie *et al.* [25] has many branches, the phenomenon of "flooding" is not obvious through the reasonable setting of the side length and angle of the spiral flow channel. Zhang found that the fin-like partition method could improve the water removal capacity of the channel. And as the number of fins increased, the effect got better [26]. Jang *et al.* [27] proposed a descending multi-channel spiral flow channel. The experimental results show that the spiral flow channel can generate secondary eddy currents, which can heighten the mass transfer effect to the GDL layer and significantly improve electrochemical performance. Similarly, Monsaf *et al.* [28] also conducted a numerical analysis of the spiral flow channel structure and found that the centrifugal force when the reaction gas flows can be adjusted by changing the number of turns of the spiral flow channel, thus improving the performance of fuel cells.

Many structures in nature can be used for references, such as small reptiles or plants. Moreover, it is not common to use animal shapes as flow channel structures, and may have unexpected benefits. Therefore, based on in-depth observation of spider shape, this paper designed a spider bionic structure including the main channel and branch channel and took the channel width/rib width and corner size of the branch channel as the research focus. This paper adopts computational fluid dynamics (CFD) software COMSOL to conduct simulation analysis on different models and compares the differences in oxygen concentration distribution, water content, and other performance of different models on the cathode side, to obtain the best numerical combination. The final scheme is compared with the common flow field, and the advanced nature of the scheme is verified.

2. Model building and parameter setting

2.1 Geometric Model

The inspiration for this design comes from the spider shape structure, and some improvements are made on this basis. In the specific geometric model shown in Fig. 1. Know from the picture, the whole flow field mainly includes the main channel and the branch channel, which is similar to the spider "leg" structure. The branch channel also has inflection points, which is helpful to promote the normal permeation of reaction gas. To make the reaction gas distribution more uniform, the inlet is set in the middle of the main channel. The cross-sectional area of the main channel is distributed in a uniform decreasing pattern from the middle to both ends, which avoids the phe-

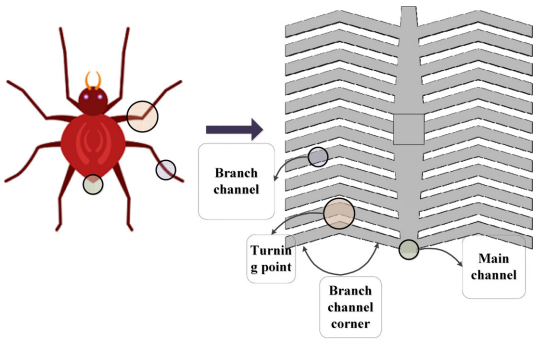

Fig. 1. Geometric model of the bionic flow channel.

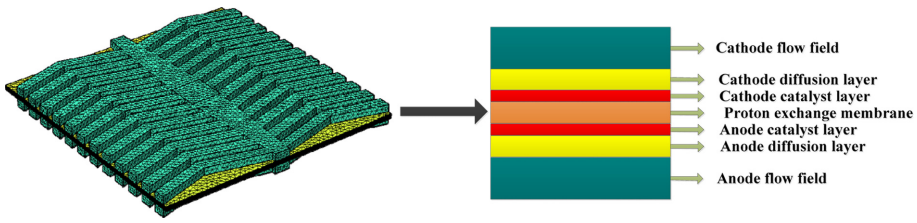

Fig. 2. Single-cell structure model of PEMFC.

Table 1. Model related parameters

Parameter	Value	Unit
Rib width	1	mm
Rib depth	1	mm
The thickness of the GDLs/CLs/membrane	0.19/0.015/0.183	mm
Branch channel depth	1	mm
Air inlet area	16	mm^2
Active area	1024	mm^2

nomenon that the reaction gas flow rate in the main channel decreases rapidly during the reaction process. As shown in Fig. 2, a complete single-cell structure model of PEMFC is constructed and simulated. Table 1 lists the geometric dimension parameters of the model. The accuracy of the above conjecture is verified through a comparative analysis of the results.

2.2 Control equations

When PEMFC is running, its internal control equations are expressed as follows [29]:

(1) The conservation of mass equation:

$$\frac{\partial(\varepsilon\rho)}{\partial t} + \nabla\cdot(\varepsilon\rho\vec{u}) = S_m \tag{1}$$

Where ρ, $\vec{u}$, ε, and S_m are the fluid density and velocity vectors, medium porosity, and quality source term, respectively. Importantly, S_m will only show up in the catalyst layer (CL) at the cathode and the anode. In the channels, $\varepsilon = 1$, $S_m = 0$ In the GDL, $\varepsilon = 0.4$, $S_m = 0$.

(2) The conservation of momentum equation:

$$\frac{\partial(\varepsilon\rho)}{\partial t} + \nabla\cdot(\varepsilon\rho\vec{u}) = -\varepsilon\nabla P + \nabla(\varepsilon\mu\nabla\vec{u}) + S_u \tag{2}$$

Where P, μ, and S_u are pressure, dynamic viscosity, and source of power, respectively. $\varepsilon = 1$ in the flow channel. Therefore, when the model is in a stable state and convection and diffusion flows in the flow field are ignored, S_u can be converted into:

$$S_u = -\frac{K_P}{\mu}\nabla P \tag{3}$$

In equation (3), K_P is the porous medium permeability.

(3) The conservation of energy equation:

$$\frac{\partial(\varepsilon\rho C_P T)}{\partial t} + \nabla\cdot(\varepsilon\rho C_P\vec{u}T) = \nabla\cdot(k^{eff}\nabla T) + S_Q \tag{4}$$

Where C_P, T, and k^{eff} are specific heat capacity (J/kg K), temperature, and effective thermal conductivity, respectively. In PEMFC, the heat source mainly includes ohmic heat, reaction heat, and polarization heat, S_Q is the energy source term.

(4) Component conservation equation:

$$\frac{\partial(\varepsilon c_k)}{\partial t} + \nabla\cdot(\varepsilon c_k\vec{u}) = \nabla\cdot(D_k^{eff}\nabla c_k) + S_k \tag{5}$$

Where D_k^{eff} is the effective diffusion coefficient of gas and S_k is the component source term, k stands for a component number. Due to the distance from the reaction region, S_k is negligible in the flow channel and GDL. For CL, the source term of each component is:

$$S_{H_2} = -\frac{1}{2F}i_a \tag{6}$$

$$S_{O_2} = -\frac{1}{4F}i_c \tag{7}$$

$$S_{H_2O} = -\frac{1}{2F}i_a \tag{8}$$

(5) Current conservation equation:

$$\nabla\cdot(k_s^{eff}\nabla\phi_s) + S_{\phi S} = 0 \tag{9}$$

$$\nabla\cdot(k_m^{eff}\nabla\phi_m) + S_{\phi m} = 0 \tag{10}$$

Where, ϕ_s and ϕ_m are solid phase and membrane phase potentials, respectively, $S_{\phi S}$ and $S_{\phi m}$ are solid phase and membrane phase current source terms respectively. According to the charge conservation principle:

$$S_{\phi m} + S_{\phi S} = 0 \tag{11}$$

(6) Equation of formation and transfer of liquid water:

The formation and transfer equation of liquid water in PEMFCs is:

$$r_w = c_r \max\left[(1-s)\frac{P_w - P_{sat}}{RT}M_{H_2O} - s\rho_l\right] \quad (12)$$

$$\frac{\partial(\varepsilon\rho_l s)}{\partial t} + \nabla(\rho_l \vec{u}_l s) = r_w \quad (13)$$

Where, r_w is water condensation rate, P_w is water vapor pressure, P_{sat} is saturated water vapor pressure, and ρ_l is water density

2.3 Model Assumptions

(1) Operating under steady-state conditions.

(2) Because the Reynolds number is less than 2000, the fluid flow is judged to be laminar.

(3) The reaction gas is fully wetted upon entry.

(4) All reaction gases are incompressible and there is no gas exchange in the membrane.

(5) Due to the uneven distribution of the material transport process, the porous medium is set to be homogeneous.

2.4 Parameter Settings

To calculate the stability of the process, it is necessary to set reasonable boundary conditions and operation parameters. The mass flow and pressure are used as the boundary at the inlet and outlet respectively. Table 2 shows the relevant parameter values [30].

2.5 Grid testing

Meshing is a key part of the simulation process. Taking the model shown in Fig. 2 as an example, different meshing methods are adopted in different domains, in which the free hexahedron structure is the main one. Table 3 shows the limiting current density values under four different grid densities. It can

Table 2. Basic parameter settings

Symbol	Numerical	Unit
Operating temperature	353.15	K
GDLs porosity	0.4	
GDLs permeability	1×10^{-13}	m^2
Reference pressure	101×10^3	Pa
The initial velocity of anode and cathode	0.3	m/s
CLs porosity	0.3	
Reference diffusion coefficient (H_2-H_2O)	1.1684×10^4	m^2/s
Reference diffusion coefficient (N_2-H_2O)	3.2682×10^5	m^2/s
Reference diffusion coefficient (O_2-H_2O)	3.5807×10^5	m^2/s
Reference diffusion coefficient (O_2-N_2)	3.0466×10^5	m^2/s
CLs permeability	2×10^{-14}	m^2
Membrane conductivity	9	S/m
Dynamic Viscosity (Anode)	1.19×10^{-5}	Pa·s
Dynamic Viscosity (Cathode)	2.46×10^{-5}	Pa·s
Initial mass fraction (H_2 Anode)	0.743	
Initial mass fraction (H_2O Cathode)	0.023	
Initial mass fraction (O_2 Cathode)	0.228	

Table 3. Influence of different mesh densities on current density

Type	#1	#2	#3	#4
Number of grids	126924	251947	336414	428564
Limiting current density (A/cm^2)	0.60869	0.70516	0.70522	0.70545

be seen that when the grid density gradient is 20~30% and the number of grids is greater than 251947, the output current is less differentiated. Therefore, it can be judged using #3 has little influence on the output result.

2.6 Validation of model rationality

Zhu *et al.* [31] measured the relevant data between voltage and current density of a 5-serpentine flow field PEMFC with professional equipment and plotted their polarization curves, where the voltage was set between 0.2 and 0.9 V. To verify the rationality of the simulation results, the same channel structure as Zhu was established and simulated. Visible able to be seen from the polarization curve shown in Fig. 3, at 0.25 V, the experimental point is farthest away from the simulation point due to the effect of temperature, environment, and other factors. At this time, the error rate is 4.17% less than 5%, so the simulation process can be considered reasonable, and this conclusion is also applicable to other model structures.

3. Results and Discussion

In PEMFC, the flow of oxygen is greatly influenced by the cathode channel. Compared with the anode, the oxygen permeability of the cathode side is poor and easily affected by the external environment. The proper design and layout of the cathode channel are very important to the effect of mass transfer and water removal. This puts forward higher requirements for the compatibility and adaptability of the flow field structure. In this section, channel width/rib width (W) and bending angle (corner) are set as variables, and the actual output effect of different types of flow channels is compared by controlling univariate and stepwise numerical variations, to find the best numerical combination.

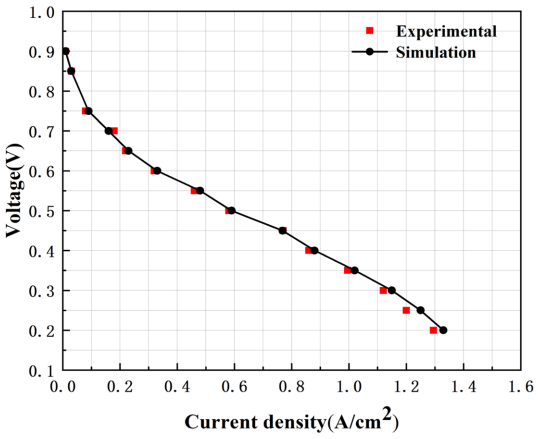

Fig. 3. Comparison curves between simulation and experimental results.

3.1 Channel width/rib width (W)

To explore the influence of the change of W value on the material transport effect and output power, PEMFC cathode channels are divided into four different types with W as a variable and 0.5 mm as a step, namely Case 1 (W = 1), Case 2 (W = 1.5), Case 3 (W = 2) and Case 4 (W = 2.5). The specific geometric dimensions are shown in Table 4.

3.1.1 Impact on PEMFC performance

In PEMFCs, in addition to distributing reactive gases and supporting the structure of the battery pack, the bipolar plate also has a very prominent contribution in collecting and conducting current. The electrons generated by the chemical reaction need to be carried through the ribs to the external circuit to prevent excess waste heat generation. The current density of PEMFC output is greatly affected by different plate sizes. When the rib size is small, the current output capacity will be weakened. Accordingly, the ability to collect conduction current is relatively weak. By contrast, if the rib width is too large, the flow channel and GDL will reduce the contact area, the phenomenon of insufficient oxygen supply to the reaction surface is easy to occur, and low oxygen concentration is also not conducive to electric currents generation, so choose the appropriate flow channel width is particularly important.

Fig. 4 shows the polarization (U-I) and power density (P-I) curves corresponding to the simulation results. Through comparative analysis, at low current density, performance curves of PEMFC with different channel types have a high degree of coincidence.

Table 4. The specific size of different W

Code	W	Corner of the numerical
Case 1	1	150°
Case 2	1.5	150°
Case 3	2	150°
Case 4	2.5	150°

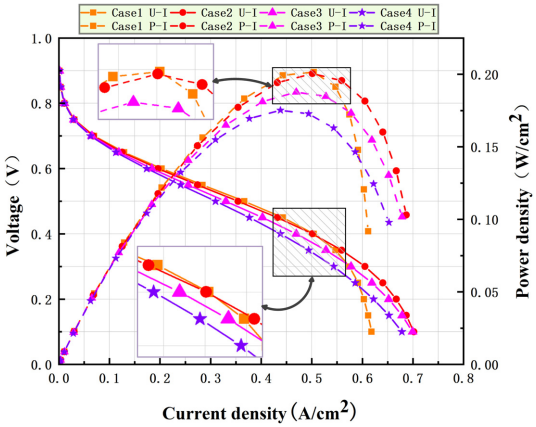

Fig. 4. U-I and P-I curves of four different PEMFC.

When the current density value is grown to over 0.2 (A/cm^2), performance curves deviate significantly. The maximum current and power density of Case 3 and 4 are below Case 2. In the reaction process, the output voltage and output power of Case 2 corresponding to the same current density are relatively large, which indicates that excessive increase of flow channel width is adverse to the generation of cell current. What is noteworthy is that when the output voltage is greater than 0.4 V, the reaction efficiency in Case 1 is maintained at a higher level. With the continuous progress of the reaction, its output performance declines rapidly, and the limiting current density value of Case 1 is the lowest among the four different types of fuel cells.

3.1.2 Oxygen mass transfer analysis

The uniformity of oxygen concentration distribution is a significant factor affecting the reaction rate of PEMFC. If the oxygen concentration in the flow channel is too low, the oxygen content reaching the GDL/CL interface will be less, which will not only affect the utilization rate of hydrogen on the anode side but also decrease the chemical reaction rate on the catalytic layer surface, directly affecting the output power of PEMFC. High oxygen concentration does not necessarily mean that output performance will be good, this is because higher oxygen concentrations correspond to higher chemical reactions, chemical reaction of hydrogen and oxygen is an exothermic process, and the severe chemical reaction will cause the GDL/CL layers in a high-temperature environment for a long time, serious when still can cause permanent damage of membrane electrode, this will greatly reduce the service life of fuel cells.

Fig. 5 depicts the comparison of the molar concentration of oxygen on the reaction surface of the four models under the operating voltage of 0.55 V. It is manifest from the figure that the oxygen concentration under the main channel is always at a high level, and the oxygen concentration does not decrease dramatically from the air inlet position to the edge of the main channel, which is mainly due to the large width of the main channel and the corresponding reduction of the resistance. Compared with the greater resistance encountered in the process of oxygen transmission in the branching channel, the corresponding permeability is stronger. As can also be observed from the figure, compared with the main channel, GDL/CL layer under the branch channel oxygen concentration decreased quickly, this phenomenon is more pronounced in branching channels away from the inlet, this is because the oxygen from the channel spreads to GDL/CL layer, constantly involved in chemical reactions to be consumed, the oxygen concentration is relatively low near the outlet of the branch channel. By comparing these four cases, it can be found that with the continuous enlargement of the W, the area of high oxygen concentration keeps

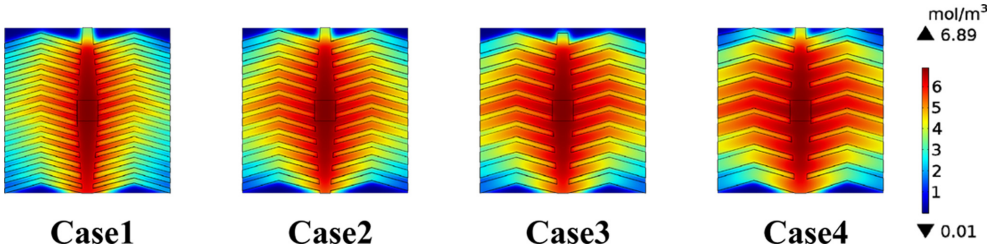

Fig. 5. Oxygen concentration of the GDL/CL interface at different W.

expanding. Compared with Case 13, the oxygen concentration distribution of Case 4 is the most uniform, indicating that the increase of the W help to enhance the infiltration capacity of oxygen into the GDL/CL layer.

3.1.3 Analysis of channel water content

Fig. 6 depicts the comparison of the molar concentration of water on the cathode channel of the four models under the operating voltage of 0.55 V. The result of the purge of the water in the cathode channel can directly affect the oxygen concentration in the chemical reaction surface. Superabundant water residue makes it difficult for oxygen to disperse along the channel, which is not conducive to the uniform distribution of oxygen in the whole flow field. The liquid water remaining in the cathode channel is mainly taken out of the flow field by the oxygen moving at high speed, so the concentration of water inside the channel is inversely proportional to the concentration of oxygen, which is consistent with the results obtained in Fig. 5.

Know from Fig. 6, the phenomenon of water aggregation at the outlet of the flow channel is serious, and this phenomenon becomes more obvious with the increase of the distance from the air inlet. This situation is mainly due to the oxygen concentration near the outlet of the flow channel is relatively thin, and the oxygen movement rate is low, so the residual water cannot be blown out of the flow channel in time. Among the four different flow channels, Case 4 has the best water removal effect compared with Case 13, indicating that a proper increase in the W can help the oxygen to obtain a higher average velocity, to destroy the accumulated aqueous solution more easily.

3.1.4 Analysis of water content in the membrane

Fig. 7 shows the water concentration distribution in the PEMFC membrane with different channel widths at 0.55 V working voltage. It is manifest from the figure that in terms of the overall distribution, Fig. 7 is similar to Fig. 6 to some extent. This is because oxygen movement speed and permeability efficiency affect water concentration in the same normal position. The control of water concentration in the membrane can directly affect the service life of the membrane and battery. If the concentration of water in the membrane is too high, the phenomenon of "flooding" will occur, which is not conducive to the infiltration of oxygen into the catalytic layer surface. Because oxygen loses electrons at the cathode side in the chemical reaction process of PEMFC, the conduction of electrons needs water as the medium. Therefore, if the oxygen concentration in the membrane is too low, it is not conducive to the generation of electric energy in the fuel cell. More importantly, if the proton exchange membrane is kept in a dry

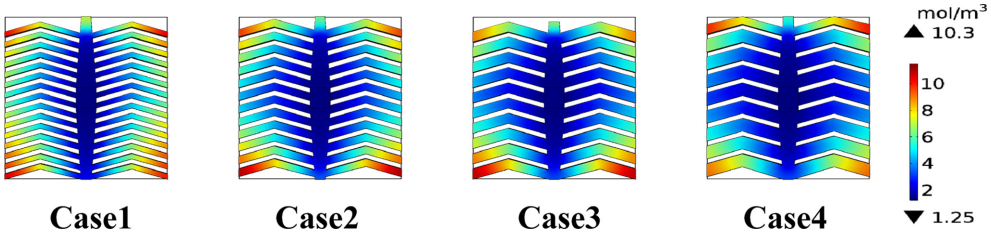

Fig. 6. Water content of the cathode channel at different W.

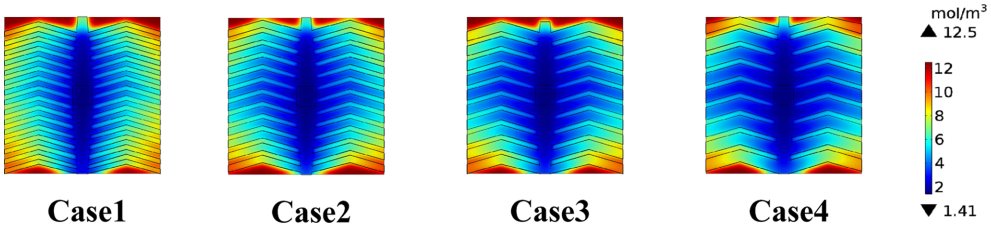

Fig. 7. Water content of the membrane at different W.

environment for a long time, it is easy to cause the membrane to dry and crack, and the service life of the fuel cell will also be greatly shortened.

It can also be observed from Fig. 7 that compared with Case 1 and 2, the water concentration in the membrane of Case 3 and 4 is relatively low, which cannot ensure the timely conversion of electrons generated by chemical reactions into the current. This is the main reason why the current density and power density of Case 3 and 4 are inferior to Case 2 even though Case 3 and 4 has a relatively uniform oxygen concentration. Compared with other types, Case 1 has the highest mean concentration of water in the membrane and can produce a large current when the oxygen supply is sufficient. Know from Fig. 5, due to the narrow width of the flow channel, the oxygen transmission effect of Case 1 is not good. Compared with Case 2~4, the oxygen concentration in the position far from the air inlet is significantly lower, which leads to a sharp decline in the chemical reaction rate. This phenomenon is also verified by the polarization and power density curve of Case 1 in Fig. 4. Therefore, after comprehensive analysis, Case 2 is the best choice among the four types.

3.2 Branch corner

The presence of inflection points in the flow channel can effectively increase the oxygen concentration at the reaction site, because the change of gas transport direction will produce a small range of eddy current, and raise the mass transfer ability of the oxygen. As can be seen from the conclusion in the previous section, when the channel width/rib width = 1.5, the fuel cell effect is better. Based on this structure, five different cases are designed, focusing on the corner at the inflection point of the branch channel. Where the change in the corner is 90~180° degrees, when the corner changes from 90 to 150°, the step length is 20°; when the corner changes from 150 to 180°, the step length is 30°. The corner change is shown in Table 4.

Table 4. Specific corner values of five cases of PEMFC

Code	Corner of the numerical
Case 5	90°
Case 6	110°
Case 7	130°
Case 2	150°
Case 8	180°

3.2.1 Impact on PEMFC performance

Under the condition that all parameters except the corner are set the same, Fig. 8 shows the polarization (U-I) and power density (P-I) curves at five different corners. The figure shows that the two performance curves differ significantly under high current density. Compared with other types, Case 7 has the highest power density value, which indicates that the output performance of fuel cells increases first and then decreases with the increasing corner. The specific reason for this phenomenon is that although the appearance of a corner can effectively improve the diffusion efficiency of reaction gas, too small a corner will not only reduce the utilization rate of the GDL/CL interface but also increase the horizontal oxygen transport resistance. In contrast, Case 7 has a slower bending corner, which not only ensures that the normal transfer capacity of the reaction gas is better than Case 8 but also ensures that the diffusion efficiency of the gas along the flow direction is better than Case 5 and 6. Can see from the above comparative analysis that the output power of the battery will not continue to increase if the branch corner is reduced all the time, which requires that it must be controlled within a certain range.

3.2.2 Oxygen mass transfer analysis

To maintain the continuous oxygen reduction reaction, it needs to be continuously supplied. Fig. 9 depicts the comparison of the molar concentration of

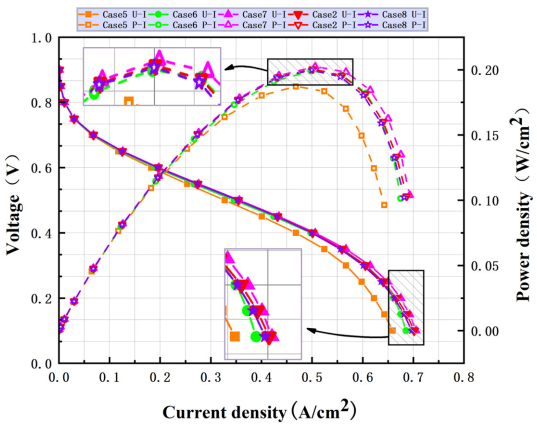

Fig. 8. U-I and P-I curves of five different flow fields.

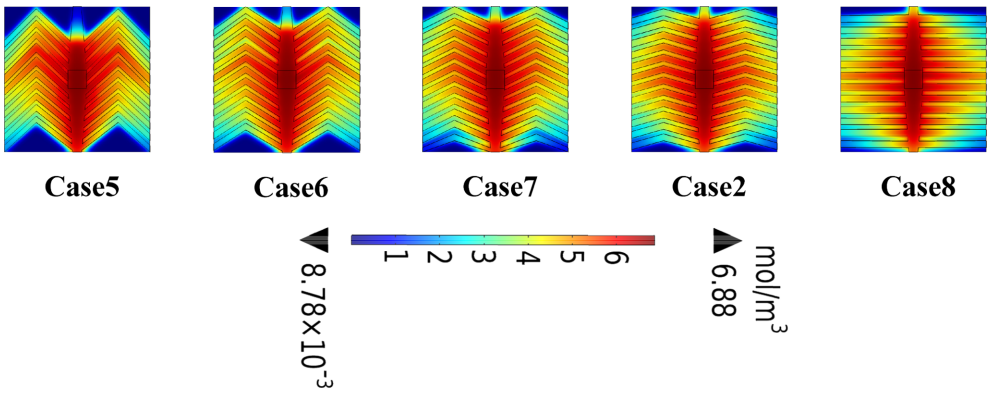

Fig. 9. Oxygen concentration of the GDL/CL interface at different corner sizes.

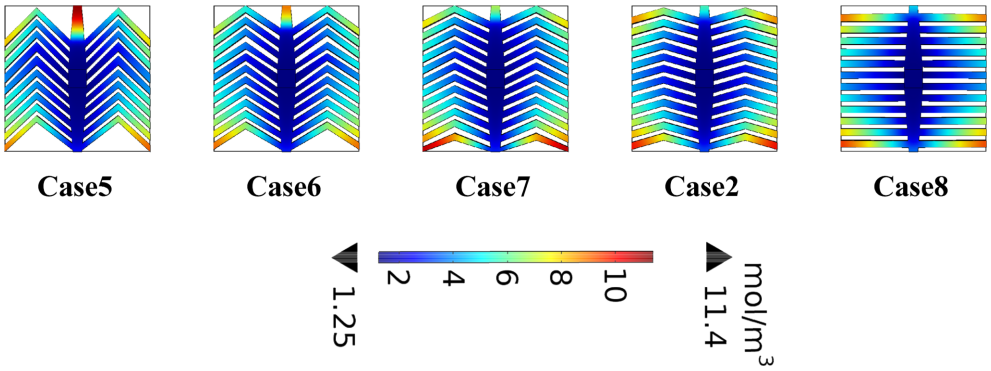

Fig. 10. Water concentration of the cathode channel at different corner sizes.

oxygen on the reaction surface of the five models under the operating voltage of 0.55 V. It is manifested from the figure that the appearance of the corner can significantly increase the area of GDL/CL layer high oxygen concentration, which is already evident in the position below the branch channel far from the air inlet. However, it can also be observed that oxygen penetration under the main channel is less effective when the corner is too small, and the area of oxygen-rich concentration is the smallest. Compared with Case 2 and 8, the oxygen distribution uniformity of the GDL/CL layer under the branch channel of Case 5~7 was significantly improved, and the overall oxygen content of the whole flow field was significantly increased. The main reason is that on the one hand, the "vortex" at the inflection point improves the permeability of oxygen; on the other hand, the "bending" phenomenon will increase the fit area between the channel and the GDL. In the position close to the air inlet, the increase of the flow channel length is conducive to the full utilization of oxygen. It can also be seen from the figure that compared with Case 7 and 8, the utilization rate of the GDL/CL layer of Case 5 and 6 is lower. Under the same plate area, the area of low oxygen concentration of Case 5 and 6 is larger, which will also reduce the output power.

3.2.3 Analysis of channel water content

Fig. 10 depicts the comparison of the molar concentration of water on the cathode channel of the five models under the operating voltage of 0.55 V. It is manifest from the figure that with the increase of the corner, the accumulation of liquid water in the branch channel becomes more and more obvious. Compared with the other four cases, Case 8 with a corner of 180° had the most moisture blockage, especially at the end of the branch channel which keeps away from the air inlet, with a water content of 11.4 mol/m^3. As the corner of Case 5 is 90°, the result of water purification in the branch channel is the best, but seri-

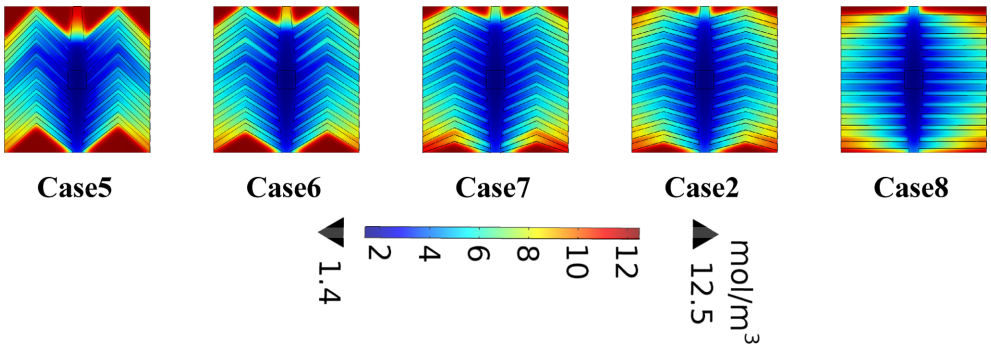

Fig. 11. Water content of the membrane at different corner sizes.

ous water accumulation occurs in the main channel. The biggest contributing factor is that the outermost part of the main channel is a one-way port, which cannot generate shunting. Besides the liquid water produced by a chemical reaction in its region that cannot be discharged in time, under the purging effect, the liquid water produced at the other locations also has a chance to flow into this area. By comprehensive comparison, it can be seen that Case 7 maintains a uniform and low water content in the whole flow field, and the optimization effect is the best.

3.2.4 Analysis of water content in the membrane

The water content at the membrane position can effectively reflect the water management efficiency of the whole cell. Fig. 11 depicts the comparison of the molar concentration of water on the membrane of the five models under the operating voltage of 0.55 V. Since the excess water in the membrane is mainly discharged from the flow field through the flow channel, Fig. 11 shows the distribution of water concentration similar to Fig. 10. In addition, from the area of the dark area, compared with the other three types, the Case 5 and 6 is more seriously differentiated. Although the water content at both ends of the membrane is sufficient, the liquid water in other areas is seriously deficient, which not only affects the output efficiency of the battery but also causes irreversible damage to the membrane. Different from Case 5 and 6, the water concentration distribution in the whole membrane region of Case 7 is more uniform. Meanwhile, compared with Case 2 and 8, the water concentration value and overall water content in the membrane region of Case 7 are higher, which is beneficial to the conduction of electrons generated by chemical reactions, thus generating a higher current density.

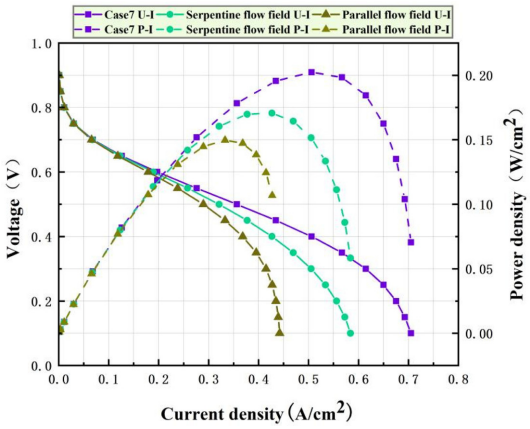

Fig. 12. Three types of PEMFC U-I and P-I curves.

3.3 Comparison with traditional flow field performance

It is found that the overall performance of case 7 is at a good level after multiple aspects of analysis. To verify the advance of this model, a comparative analysis is made between Case 7 and traditional parallel and serpentine channel fuel cells. In this process, other irrelevant quantities (flow channel width and height, etc.) except the flow channel mode are guaranteed to be the same.

Fig. 12 emerges the corresponding U-I and P-I curves of PEMFC with different structures. We can see that Case 7 significantly improves the output power of the battery compared with parallel and serpentine structures. Fig. 13 shows the state of oxygen and water at the GDL/CL interface and in the channel at 0.55 V voltage. As shown in the illustration, there is little difference in oxygen concentration within the three flow fields, but the Parallel channel and the serpentine flow channel have smaller areas of high oxy-

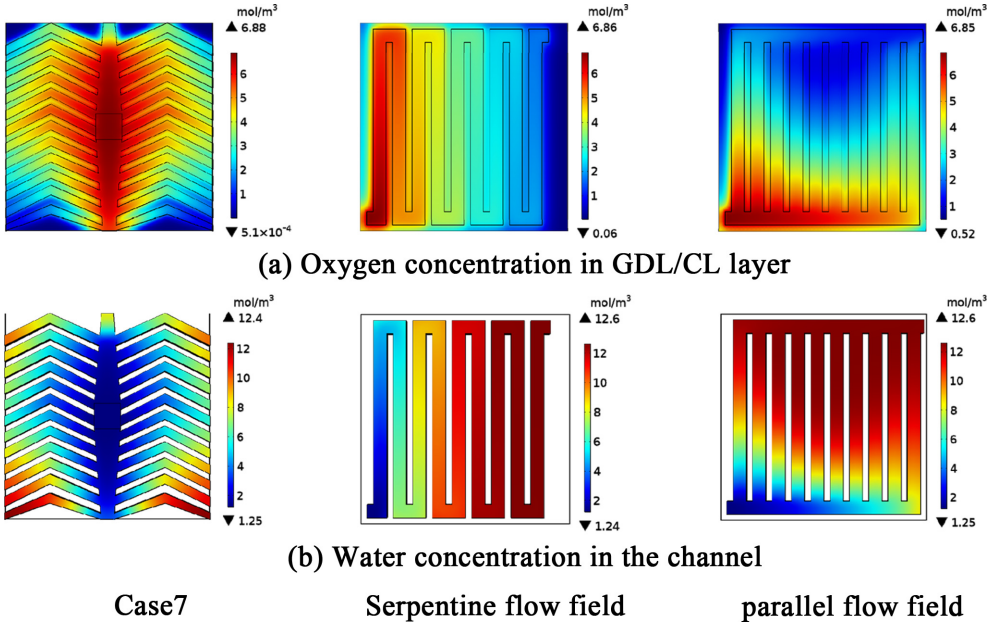

Fig. 13. Different flow channel types for (a) oxygen content at the GDL/CL interface and (b) water content in the cathode channel.

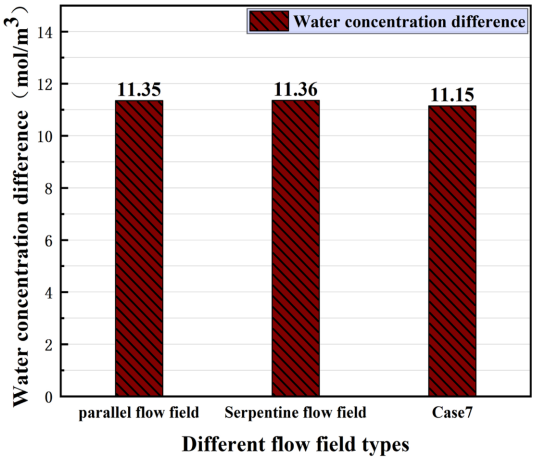

Fig. 14. Differences in water concentration in different flow channels.

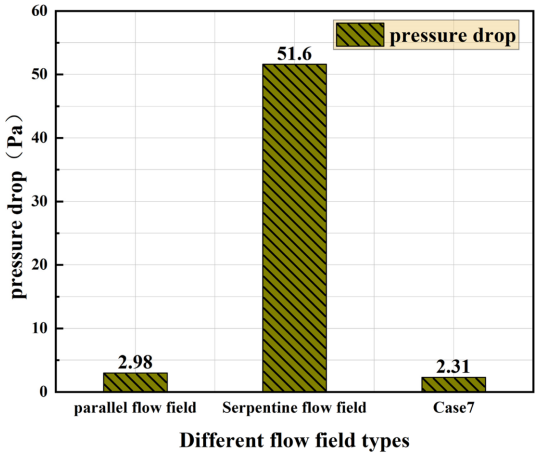

Fig. 15. Comparison of pressure drop of different flow channels.

gen concentration, and the oxygen concentration drops faster. Fig. 14 emerges the difference in water molar concentration in three different cathode channels. As shown in the illustration, like the oxygen distribution, the water concentration in the different channels varied by less than 0.3 mol/m^3. It is manifest from Fig. 13 that the area of high-water content in the parallel channel and the serpentine channel is large, indicating that serious "water blockage" occurs in both of them under the same conditions. Fig. 15 emerges the three-cathode channel pressure drops. It can be found that the pressure drop value of the serpentine channel is much higher than that of the other two types. The high-pressure drop means that more pumping power is consumed. As can be seen from the above, the overall performance of Case 7 is better than that of traditional flow channels.

4. Conclusions

In this paper, based on the in-depth observation of spider shape, a new bionic flow channel is designed. Under the premise of keeping the main channel area unchanged, through CFD simulation to discuss the influence of the branch channel parameters on the output performance of the battery.

Reducing the channel width appropriately is an appropriate choice. Of the four types compared, Case 2 (W = 1.5) had the highest power density value. Conversely, Case 4 (W = 2.5) had the lowest power output, with a 13.23% reduction in maximum power density compared to Case 2. In oxygen concentration distribution, as the W increases, the high oxygen concentration area expands unceasingly, water concentration distribution of the contrary. However, in general, the total oxygen content of the Case 2 GDL/CL layer and the total water content in the membrane is better than Case 3 and 4, which is beneficial to the wetting and chemical reaction of the membrane.

On the other hand, the corner size of the branch channel is an important factor. Among the five different corner fuel cells, Case 7 (corner = 130°) has the highest output power (0.1984 W/cm^2), the overall oxygen content is higher than Case 2 and 8, and the oxygen concentration distribution uniformity is better than Case 5 and 6, and the water concentration distribution uniformity is better than the other four types. The above analysis shows that the best combination effect is the channel width/rib width = 1.5 and the branch corner = 130°.

Disclosure statement

None of the participants in this article has any dispute of interest.

Funding

Thanks for the support of the Shandong Provincial major science and technology innovation project (2018-CXGC0803).

References

[1] G. Zhang, L. Guo, B. Ma, and H. Liu, *J. Power Sources*, **2009**, *188(1)*, 213-219.
[2] X. Zeng, Y. Ge, J. Shen, L. Zeng, Z. Liu, and W. Liu, *Int. J. Heat Mass Transfer*, **2017**, *105*, 81-89.
[3] K. Xiong, W. Wu, S. Wang, and L. Zhang, *Appl. Energy*, **2021**, *301*, 117443.
[4] L. Xia, Z. Yu, G. Xu, S. Ji, and B. Sun, *Energy Convers. Manage.*, **2021**, *247*, 114707.
[5] C.-T. Wang, Y.-T. Ou, B.-X. Wu, S. Thangavel, S.-W. Hong, W.-T. Chung, and W.-M. Yan, *Energy Procedia*, **2017**, *142*, 667-673.
[6] Q. Tan, H. Lei, and Z. Liu, *Int. J. Hydrog. Energy*, **2022**, *47(23)*, 11975-11990.
[7] C.-T. Wang, Y.-C. Hu, and P.-L. Zheng, *Appl. Energy*, **2010**, *87(4)*, 1366-1375.
[8] M. K. Vijayakrishnan, K. Palaniswamy, J. Ramasamy, T. Kumaresan, K. Manoharan, T. K. R. Rajagopal, T. Maiyalagan, V. R. Jothi, and S. C. Yi, *Int. J. Hydrog. Energy*, **2020**, *45(13)*, 7848-7862.
[9] V. H. Rangel-Hernandez, C. Damian-Ascencio, D. Juarez-Robles, A. Gallegos-Muñoz, A. Zaleta-Aguilar, and H. Plascencia-Mora, *Energy*, **2011**, *36(8)*, 4864-4870.
[10] S. Liu, T. Chen, Y. Xie, J. Zhang, and C. Wu, *Int. J. Hydrog. Energy*, **2019**, *44(56)*, 29618-29630.
[11] M. Liu, H. Huang, X. Li, X. Guo, T. Wang, and H. Lei, *Int. J. Hydrog. Energy*, **2021**, *46(75)*, 37379-37392.
[12] F. Liu, M. Kvesić, K. Wippermann, U. Reimer, and W. Lehnert, *J. Electrochem. Soc.*, **2013**, *160(8)*, F892-F897.
[13] S. B. Li and Y. L. Liu, *Appl. Mech. Mater.*, **2011**, *63-64*, 365-368.
[14] M. Marappan, K. Palaniswamy, T. Velumani, K. B. Chul, R. Velayutham, P. Shivakumar, and S. Sundaram, *Chem. Rec.*, **2021**, *21(4)*, 663-714.
[15] M. Sauermoser, N. Kizilova, B. G. Pollet, and S. Kjelstrup, *Front. Energy Res.*, **2020**, *8*, 13.
[16] T. Chen, Y. Xiao, and T. Chen, *Energy Procedia*, **2012**, *28*, 134-139.
[17] H. Huang, H. Lei, M. Liu, T. Wang, C. Li, X. Guo, Y. Chen, and M. Pan, Energy Convers. Manag., 2020, 226, 113546.
[18] J. P. Kloess, X. Wang, J. Liu, Z. Shi, and L. Guessous, *J. Power Sources*, **2009**, *188*, 132-140.
[19] D. K. Dang and B. Zhou, *Int. J. Energy Res.*, **2021**, *45(14)*, 20285-20301.
[20] A. Iranzo, C. H. Arredondo, A. M. Kannan and F. Rosa, *Energy*, **2020**, *190*, 116435.
[21] S. Zhang, H. Xu, Z. Qu, S. Liu and F. K. Talkhoncheh, *J. Power Sources*, **2022**, *522*, 231003.
[22] S. R. Badduri, G. N. Srinivasulu, and S. S. Rao, *Chin. J. Chem. Eng.*, **2020**, *28(3)*, 824-831.
[23] T. Chen, Y. Xiao, and T. Chen. *Energy Procedia*, **2012**, *28*, 134-139.
[24] S. Zhang, S. Liu, H. Xu, G. Liu, and K. Wang, *Energy*, **2022**, *239*, 122102.
[25] Q. Xie and M. Zheng, *Processes*, **2021**, *9(9)*, 1526.
[26] S. Y. Zhang, Z. G. Qu, H. T. Xu, F. K. Talkhoncheh, S. Liu, and Q. Gao, *Int. J. Hydrog. Energy*, **2021**, *46(54)*, 27700-27708.
[27] J. Y. Jang, C. H. Cheng, W. T. Liao, Y. X. Huang, and Y.

C. Tsai, *Appl. Energy*, **2012**, *99*, 67-79.
[28] T. Monsaf, B. M. Hocine, S. Youcef, and M. Abdallah, *Int. J. Hydrog. Energy*, **2017**, *42(2)*, 1237-1251.
[29] S. H. Han, N. H. Choi, and Y. D. Choi, *Int. J. Hydrog. Energy*, **2014**, *39(6)*, 2628-2638.
[30] M. Z. Chowdhury and B.Timurkutluk, *Energy*, **2018**, *161*, 104-117.
[31] W. Zhu and M. Zheng, *Int. J. Heat Technol.*, **2019**, *37(3)*, 733-740.